Inorganic Chemistry
Article

Inorg. Chem. **2009**, *48*, 11067–11078 **11067**
DOI: 10.1021/ic901429u

Self-Assembly of Metal-Organic Coordination Polymers Constructed from a Bent Dicarboxylate Ligand: Diversity of Coordination Modes, Structures, and Gas Adsorption

Wenbin Yang, Xiang Lin, Alexander J. Blake, Claire Wilson, Peter Hubberstey, Neil R. Champness,* and Martin Schröder*

School of Chemistry, University of Nottingham, University Park, Nottingham NG7 2RD, U.K.

Received July 22, 2009

We have synthesized five new metal-organic coordination polymers incorporating the bent ligand H_2hfipbb [4,4′-(hexafluoroisopropylidene)bis(benzoic acid)] with different transition metal ions and co-ligands via solvothermal reactions to give $[Zn_2(hfipbb)_2(py)_2]\cdot DMF$ (**1**), $[Zn_2(hfipbb)_2(4,4'\text{-bipy})(H_2O)]$ (**2**), $[Zn_2(hfipbb)_2(bpdab)]\cdot 2DMF$ (**3**), $[Cd_2(hfipbb)_2(DMF)_2]\cdot 2DMF$ (**4**), and $[Co(hfipbb)(dpp)]\cdot MeOH$ (**5**) (py = pyridine, 4,4′-bipy = 4,4′-bipyridine, bpdab = 1,4-bis(4-pyridyl)-2,3-diaza-1,3-butadiene, dpp = 1,3-di(4-pyridyl)propane). Compound **1** displays a 2-fold 2D→2D parallel interpenetrated layer network with one-dimensional (1D) helical channels, while **3** exhibits a three-dimensional pillared helical-layer open framework of α-Po topology based upon binuclear paddlewheel units. In compounds **2** and **5**, binuclear motifs with double carboxylate bridges are linked by $hfipbb^{2-}$ ligands into a 1D ribbon, which are further assembled into two-dimensional non-interpenetrated (4,4) layers via bipyridyl co-ligands. However, the different bridging modes of $hfipbb^{2-}$ ligands and the different disposition of the coordinated co-ligands around metal ions result in subtle differences in the final architecture. Thus, **2** is based on a binuclear cluster node, double-stranded $hfipbb^{2-}$ linkers, and single-stranded 4,4′-bipy linkers, while **5** is based on a binuclear cluster node and $hfipbb^{2-}$ and dpp linkers which are both double-stranded. Among these compounds, the Cd(II) complex **4** is possibly the most interesting because it represents a rare example in which metal centers are linked by carboxylate groups into infinite chains further joined together by $hfipbb^{2-}$ spacers to form a 2D network with tubular helical channels. All these coordination polymers exhibit low solvent-accessible volumes. Both **3** and **4** retain structural integrity and permanent microporosity upon evacuation of guest molecules, with hydrogen uptakes of 0.57 and 0.78 wt %, respectively, at 20 bar and 77 K.

Introduction

The design and synthesis of metal-organic coordination polymers have drawn significant interest in recent years,[1] not only for their structural diversity and intriguing molecular topologies[2,3] but also for their potential as a new class of porous materials applied in the fields of separation,[4]

*To whom correspondence should be addressed. E-mail: m.schroder@nottingham.ac.uk (M.S.), neil.champness@nottingham.ac.uk (N.R.C.). Phone: +44 (0)115 9513490. Fax: +44 (0)115 9513563.

(1) For reviews on metal-organic frameworks and coordination polymers see: (a) Mueller, U.; Schubert, M.; Teich, F.; Puetter, H.; Schierle-Arndt, K.; Pastre, J. *J. Mater. Chem.* **2006**, *16*, 626. (b) Kitagawa, S.; Noro, S. J.; Nakamura, T. *Chem. Commun.* **2006**, 701. (c) Kitagawa, S.; Uemura, K. *Chem. Soc. Rev.* **2005**, *34*, 109. (d) Kitagawa, S.; Kitaura, R.; Noro, S. I. *Angew. Chem., Int. Ed.* **2004**, *43*, 2334. (e) Zhou, Y. F.; Hong, M. C.; Wu, X. T. *Chem. Commun.* **2006**, 135. (f) Brammer, L. *Chem. Soc. Rev.* **2004**, *33*, 476. (g) Dobrawa, R.; Wuerthner, F. *J. Polym. Sci., Part A: Polym. Chem.* **2005**, *43*, 4981. (h) Uemura, K.; Matsuda, R.; Kitagawa, S. *J. Solid State Chem.* **2005**, *178*, 2420. (i) Moulton, B.; Zaworotko, M. *J. Chem. Rev.* **2001**, *101*, 1629. (j) Blake, A. J.; Champness, N. R.; Hubberstey, P.; Li, W.-S.; Withersby, M. A.; Schroder, M. *Coord. Chem. Rev.* **1999**, *183*, 117. (k) Dincă, M.; Long, J. R. *Angew. Chem., Int. Ed.* **2008**, *47*, 6766. (l) Lin, X.; Jia, J.; Hubberstey, P.; Schröder, M; Champness, N. R. *CrystEngComm* **2007**, *9*, 438. (m) Murray, L. J.; Dincă, M.; Long, J. R. *Chem. Soc. Rev.* **2009**, *38*, 1294. (n) Wang, Z.; Cohen, S. *Chem. Soc. Rev.* **2009**, *38*, 1315. (o) Shimizu, G. K. H.; Vaidhyanathan, R.; Taylor, J. M. *Chem. Soc. Rev.* **2009**, *38*, 1430. (p) Li, J.-R.; Kuppler, R. J.; Zhou, H.-C. *Chem. Soc. Rev.* **2009**, *38*, 1477. (q) Uemura, T.; Yanai, N.; Kitagawa, S. *Chem. Soc. Rev.* **2009**, *38*, 1228. (r) Czaja, A. U; Trukhan, N.; Müller, U. *Chem. Soc. Rev.* **2009**, *38*, 1284.

(2) (a) Hill, R. J.; Long, D. L.; Hubberstey, P.; Champness, N. R.; Schröder, M. *Acc. Chem. Res.* **2005**, *38*, 337. (b) O'Keeffe, K.; Eddaoudi, M.; Li, H.; Reineke, T.; Yaghi, O. M. *J. Solid State Chem.* **2000**, *152*, 3. (c) Champness, N. R.; Schröder, M. *Curr. Opin. Solid State Mater. Sci.* **1998**, *3*, 419. (d) Hill, R. J.; Long, D.-L.; Hubberstey, P.; Schröder, M.; Champness, N. R. *J. Solid State Chem.* **2005**, *178*, 2414. (e) Long, D.-L.; Hill, R. J.; Blake, A. J.; Champness, N. R.; Hubberstey, P.; Wilson, C.; Schröder, M. *Chem.—Eur. J.* **2005**, *11*, 1384.

(3) (a) Robin, A. Y.; Fromm, K. M. *Coord. Chem. Rev.* **2006**, *250*, 2127. (b) Champness, N. R. *Dalton Trans.* **2006**, 877. (c) Blake, A. J.; Champness, N. R.; Cooke, P. A.; Hubberstey, P.; Realf, A. L.; Schröder, M. *J. Chem. Soc., Dalton Trans.* **2000**, 3261. (d) Blake, A. J.; Brooks, N. R.; Champness, N. R.; Crew, M.; Hanton, L. R.; Hubberstey, P.; Parsons, S.; Schröder, M. *J. Chem. Soc., Dalton Trans.* **1999**, 2813. (e) Long, D.-L.; Blake, A. J.; Champness, N. R.; Schröder, M. *Chem. Commun.* **2000**, 2273. (f) Blake, A. J; Champness, N. R.; Crew, M.; Hanton, L. H.; Parsons, S.; Schröder, M. *J. Chem. Soc., Dalton Trans.* **1998**, 1533.

(4) (a) Chen, B.; Liang, C.; Yang, J.; Contreras, D. S.; Clancy, Y. L.; Lobkovsky, E. B.; Yaghi, O. M.; Dai, S. *Angew. Chem., Int. Ed.* **2006**, *45*, 1390. (b) Choi, H. J.; Suh, M. P. *J. Am. Chem. Soc.* **2004**, *126*, 15844. (c) Pan, L.; Olson, D. H.; Ciemnolonski, L. R.; Heddy, R.; Li, J. *Angew. Chem., Int. Ed.* **2006**, *45*, 616.

Published on Web 10/30/2009

heterogeneous catalysis,[5] gas storage,[6] and drug delivery.[7] The structures of coordination polymers are dependent upon a variety of factors such as the geometrical and electronic properties of the metal ions used, the bulk and coordinative abilities of the ligands, the ligand-to-metal stoichiometry, and the use of different solvents, synthetic strategies, and methods of crystal growth. In particular, variation of ligand conformations often plays a key role in the self-assembly processes to give metal-organic coordination polymers with different structural topologies. By adjusting the shape, functionality, flexibility, length, and symmetry of the spacers, a remarkable range of materials containing various architectures and functions can be prepared.[1,8−11]

Carboxylate O-donors have the ability to coordinate to metal centers in a variety of modes, ranging from mono- or *bis*-chelate fashion to μ^3-η^2:η, μ^4-η^2:η^2, and μ^5-η^3:η^3 bridging modes.[9−13] The wide variety of coordination modes of carboxylates and their high affinity for metal ions give metal carboxylate complexes a rich structural chemistry. In addition, the carboxylate unit can bind together with a phosphate group or an N-containing heterocycle to give intriguing hybrid structures.[14] Thus, polycarboxylate ligands, in particular, aromatic di- and multibranched carboxylates (i.e., terephthalic, isophthalic, trimesic, and pyromellitic acid) and various pyridine- and imidazole-dicarboxylates, have been widely used in the rational design of metal-organic coordination polymers.[9−18] Recently, strategies have been reported using combinations of appropriate *N,N′*-donor bidentate ligands to introduce pillars to link well-defined two-dimensional (2D) metal-carboxylate layers.[19] In this way the structures of a wide variety of coordination polymers can be predicted, and the pore size and chemical functionality of the resultant open frameworks readily controlled via a modification of the pillars.[20] One of the best-known examples is the series $[M_2(2,3\text{-pyzdc})_2L_{pillar}]_n$ [M = Cu and Cd; 2,3-pyzdc^{2-} = pyrazine-2,3-dicarboxylate; L_{pillar} = pyrazine, 4,4′-bipyridine, 1,2-di(4-pyridyl)glycol, 1,4-diazabicyclo[222]-octane, and py-N═N-py/py-CH═CH-py (py = pyridin-4-yl)].[20,21] These microporous materials incorporate pillar ligand bridges between the neutral layers of $[M_2(2,3\text{-pyzdc})_2]_n$. Other examples of porous pillar-layered architectures are based upon binuclear paddlewheel building blocks bridged by linear anionic dicarboxylates to form 2D square grids further extended by various neutral *N,N′*-donor pillars to give three-dimensional (3D) α-Po porous structures with one-dimensional (1D) channels.[19,22] Some of these layer-pillared architectures display a degree of hydrogen storage capacity.[19,22a−c]

We report herein the use of the commercially available 4,4′-(hexafluoroisopropylidene)bis(benzoic acid) (H_2hfipbb) as a tecton in the synthesis of novel coordination frameworks. The hfipbb^{2-} ligand incorporates a C(sp^3) fluorinated spacer which forces it to be bent, thus enhancing the potential

(5) (a) Wu, C. D.; Hu, A.; Lin, W. B. *J. Am. Chem. Soc.* **2005**, *127*, 8940. (b) Uemara, T.; Kitagawa, K.; Horike, S.; Kawamura, T.; Kitagawa, S. *Chem. Commun.* **2005**, 5868. (c) Fujita, M.; Kwon, Y. J.; Washizu, S.; Ogura, K. J. *J. Am. Chem. Soc.* **1994**, *116*, 1151. (d) Gomez-lor, B.; Gutiérrez-Puebla, E.; Iglesias, M.; Monge, M. A.; Ruiz-Valero, C.; Snejko, N. *Inorg. Chem.* **2002**, *41*, 2429. (e) Tanski, J. M.; Wolczanski, P. T. *Inorg. Chem.* **2001**, *40*, 2026. (f) Seo, J. S.; Whang, D.; Lee, H.; Jun, S. I.; Oh, J.; Jeon, Y. J.; Kim, K. *Nature* **2000**, *404*, 982.

(6) (a) Kesanli, B.; Cui, Y.; Smith, M. R.; Bittner, E. W.; Bockrath, B. L.; Lin, W. *Angew. Chem., Int. Ed.* **2005**, *44*, 72. (b) Panella, B.; Hirscher, M. *Adv. Mater.* **2005**, *17*, 538. (c) Pan, L.; Liu, H. R.; Lei, X.; Huang, X.; Olson, D. H.; Turro, N. J.; Li, J. *Angew. Chem., Int. Ed.* **2003**, *42*, 542. (d) Zhao, X.; Xiao, B.; Fletcher, A. J.; Thomas, K. M.; Bradshaw, D.; Rosseinsky, M. J. *Science* **2004**, *306*, 1012. (e) Zhao, B.; Chen, X. Y.; Cheng, P.; Liao, D. Z.; Yan, S. P.; Jiang, Z. H. *J. Am. Chem. Soc.* **2004**, *126*, 15394. (f) Pan, L.; Sander, M. B.; Huang, X.; Li, J.; Smith, M.; Bittner, E.; Bockrath, B.; Johnson, J. K. *J. Am. Chem. Soc.* **2004**, *126*, 1308. (g) Yang, S.; Lin, X.; Blake, A. J.; Thomas, K. M.; Hubberstey, P.; Champness, N. R.; Schröder, M. *Chem. Commun.* **2008**, 6108. (h) Yan, Y.; Lin, X.; Yang, S.; Blake, A. J.; Dailly, A.; Champness, N. R.; Hubberstey, P.; Schröder, M. *Chem. Commun.* **2009**, 1025. (i) Lin, X.; Telepeni, I.; Blake, A. J.; Dailly, A.; Brown, C. M.; Simmons, J. M.; Zoppi, M.; Walker, G. S.; Thomas, K. M.; Mays, T. J.; Hubberstey, P.; Champness, N. R.; Schröder *J. Am. Chem. Soc.* **2009**, *131*, 2159. (j) Yang, S.; Lin, X.; Dailly, A.; Blake, A. J.; Champness, N. R.; Hubberstey, P.; Schröder, M. *Chem.—Eur. J.* **2009**, *15*, 4829. (k) Yang, S.; Lin, X.; Blake, A. J.; Walker, G. S.; Hubberstey, P.; Champness, N. R.; Schröder, M. *Nat. Chem.,* **2009**, *1*, 487.

(7) (a) Horcajada, P.; Serre, C.; Maurin, G.; Ramsahye, N. A.; Balas, F.; Vallet-Regí, M.; Sebban, M.; Taulelle, F.; Férey, G. *J. Am. Chem. Soc.* **2008**, *130*, 6774. (b) Horcajada, P.; Serre, C.; Vallet-Regí, M.; Sebban, M.; Taulelle, F.; Férey, G. *Angew. Chem., Int. Ed.* **2006**, *45*, 5974.

(8) (a) Kesanli, B.; Lin, W. *Coord. Chem. Rev.* **2003**, *246*, 305. (b) Kiang, Y.-H.; Gardner, G. B.; Lee, S.; Xu, Z.; Lobkovsky, E. B. *J. Am. Chem. Soc.* **1999**, *121*, 8204.

(9) (a) Li, H.; Eddaoudi, M.; O'Keeffe, M.; Yaghi, O. M. *Nature* **1999**, *402*, 276. (b) Rowsell, J. L. C.; Millward, A. R.; Park, K. S.; Yaghi, O. M. *J. Am. Chem. Soc.* **2004**, *126*, 5666. (c) Rosi, N. L.; Eckert, J.; Eddaoudi, M.; Vodak, D. T.; Kim, J.; O'Keeffe, M.; Yaghi, O. M. *Science* **2003**, *300*, 1127.

(10) (a) Furukawa, S.; Hirai, K.; Nakagawa, K.; Takashima, Y.; Matsuda, R.; Tsuruoka, T.; Kondo, M.; Haruki, R.; Tanaka, D.; Sakamoto, H.; Shimomura, S.; Sakata, O.; Kitagawa, S. *Angew. Chem., Int. Ed.* **2009**, *48*, 1766. (b) Ghosh, S. K.; Kaneko, W.; Kiriya, D.; Ohba, M.; Kitagawa, S. *Angew. Chem., Int. Ed.* **2008**, *47*, 8843.

(11) (a) Cairns, A. J.; Perman, J. A.; Wojtas, L.; Kravtsov, V. C.; Alkordi, M. H.; Eddaoudi, M.; Zaworotko, M. J. *J. Am. Chem. Soc.* **2008**, *130*, 1560. (b) Perry, J. J.; Kravtsov, V. C.; McManus, G. J.; Zaworotko, M. J. *J. Am. Chem. Soc.* **2007**, *129*, 10076.

(12) (a) Anokhina, E. V.; Vougo-Zanda, M.; Wang, X.; Jacobson, A. J. *J. Am. Chem. Soc.* **2005**, *127*, 15000. (b) Pan, L.; Parker, B.; Huang, X. Y.; David, D. H.; lee, J. Y.; Li, J. *J. Am. Chem. Soc.* **2006**, *128*, 4180.

(13) (a) Kim, J.; Chen, B.; Reineke, T. M.; Li, H.; Eddaoudi, M.; Moler, D. B.; O'Keeffe, M.; Yaghi, O. M. *J. Am. Chem. Soc.* **2001**, *123*, 8239. (b) Majumder, A.; Gramlich, V.; Rosair, G. M.; Batten, S. R.; Masuda, J. D.; El Fallah, M. S.; Ribas, J.; Sutter, J. P.; Desplanches, C.; Mitra, S. *Cryst. Growth Des.* **2006**, *6*, 2355.

(14) (a) Shi, X.; Zhu, G. S.; Qiu, S. L.; Huang, K. L.; Yu, J. H.; Xu, R. R. *Angew. Chem., Int. Ed.* **2004**, *43*, 6482. (b) Gutschke, S. O. H.; Price, D. J.; Powell, A. K.; Wood, P. T. *Angew. Chem., Int. Ed.* **1999**, *39*, 1088. (c) Yang, W.; Lin, X.; Jia, J.; Blake, A. J.; Wilson, C.; Hubberstey, P.; Champness, N. R.; Schröder, M. *Chem. Commun.* **2008**, 359.

(15) (a) Jia, J.; Lin, X.; Blake, A. J.; Champness, N. R.; Hubberstey, P.; Shao, L.; Walker, G.; Wilson, C.; Schröder, M. *Inorg. Chem.* **2006**, *45*, 8838. (b) Jia, J.; Lin, X.; Wilson, C.; Blake, A. J.; Champness, N. R.; Hubberstey, P.; Walker, G.; Cussen, E. J.; Schröder, M. *Chem. Commun.* **2007**, 840.

(16) Zhang, X. M.; Zheng, Y. Z.; Li, C. R.; Zhang, W. X.; Chen, X. M. *Cryst. Growth Des.* **2007**, *7*, 980.

(17) Huang, Y. G.; Wu, B. L.; Yuan, D. Q.; Xu, Y. Q.; Jiang, F. L.; Hong, M. C. *Inorg. Chem.* **2007**, *46*, 1171.

(18) (a) Qing, C.; Wang, X. L.; Wang, E. B.; Su, Z. M. *Inorg. Chem.* **2005**, *44*, 7122. (b) Zhang, G. Q.; Wang, Q.; Qian, Y.; Yang, G. Q.; Ma, J. S. *J. Mol. Struct.* **2006**, *796*, 187.

(19) (a) Chen, B. L.; Ma, S. Q.; Zapata, F.; Lobkovsky, E. B.; Yang, J. *Inorg. Chem.* **2006**, *45*, 5718. (b) Chun, H.; Dybtsev, D. N.; Kim, H.; Kim, K. *Chem.—Eur. J.* **2005**, *11*, 3521.

(20) (a) Li, C. J.; Hu, S.; Li, W.; Lam, C. K.; Zheng, Y. Z.; Tong, M. L. *Eur. J. Inorg. Chem.* **2006**, 1931. (b) Kitaura, R.; Fujimoto, K.; Noro, S. I.; Kondo, M.; Kitagawa, S. *Angew. Chem., Int. Ed.* **2002**, *41*, 133.

(21) (a) Maji, T. K.; Uemura, K.; Chang, H. C.; Matsuda, R.; Kitagawa, S. *Angew. Chem., Int. Ed.* **2004**, *43*, 3629. (b) Matsuda, R.; Kitaura, R.; Kitagawa, S.; Kubota, Y.; Belosludov, R. V.; Kobayashi, T. C.; Sakamoto, H.; Chiba, T.; Takata, M.; Kawazoe, Y.; Mita, Y. *Nature* **2005**, *436*, 238.

(22) (a) Kitaura, R.; Iwahori, F.; Matsuda, R.; Kitagawa, S.; Kubota, Y.; Takata, M.; Kobayashio, T. C. *Inorg. Chem.* **2004**, *43*, 6533. (b) Dybtsev, D. N.; Chun, H.; Kim, K. *Angew. Chem., Int. Ed.* **2004**, *43*, 5033. (c) Mulfort, K. L.; Farha, O. K.; Stern, C. L.; Sarjeant, A. A.; Hupp, J. T. *J. Am. Chem. Soc.* **2009**, *131*, 3886. (d) Ma, B. -Q.; Mulfort, K. L.; Hupp, J. T. *Inorg. Chem.* **2005**, *44*, 4912. (e) Shultz, A. M.; Farha, O. K.; Hupp, J. T.; Nguyen, S. T. *J. Am. Chem. Soc.* **2009**, *131*, 4204. (f) Bae, Y.-S.; Mulfort, K. L.; Frost, H.; Ryan, P.; Punnathanam, S.; Broadbelt, L. J.; Hupp, J. T.; Snurr, R. Q. *Langmuir* **2008**, *24*, 8592.

Scheme 1. Schematic Representation of the Diverse Structures Observed in **1**−**5**[a]

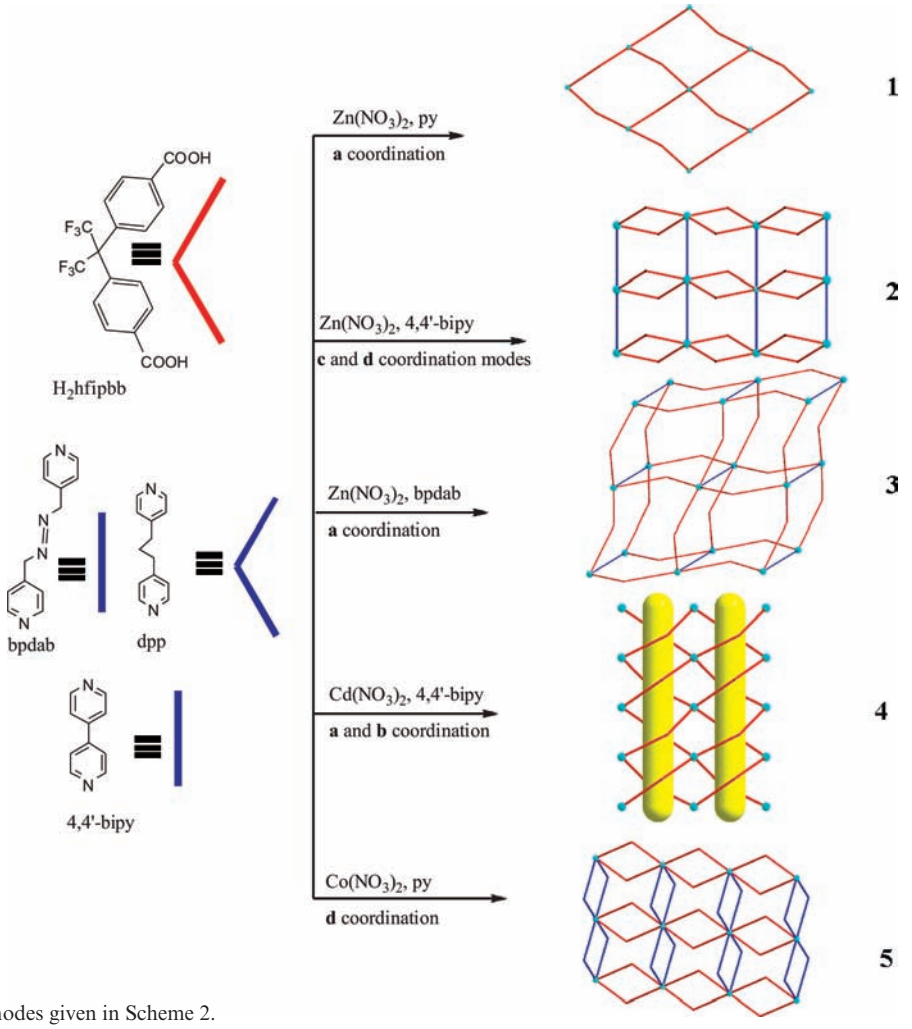

[a] a−d coordination modes given in Scheme 2.

formation of helical and self-penetrating networks. This semirigid molecule has been shown previously to bridge different transition and rare-earth metal ions to give materials with interesting sorption, catalytic, luminescent, or magnetic properties.[4c,6f,23] Under appropriate synthetic conditions and in the presence of auxiliary co-ligands, five new coordination polymers, $[Zn_2(hfipbb)_2(py)_2]\cdot DMF$ (**1**), $[Zn_2(hfipbb)_2(4,4'\text{-bipy})(H_2O)]$ (**2**), $[Zn_2(hfipbb)_2(bpdab)]\cdot 2DMF$ (**3**), $[Cd_2(hfipbb)_2(DMF)_2]\cdot 2DMF$ (**4**), and [Co(hfipbb)(dpp)]·MeOH (**5**) (py = pyridine, 4,4′-bipy = 4,4′-bipyridine, bpdab = 1,4-bis(4-pyridyl)-2,3-diaza-1,3-butadiene, dpp = 1,3-di(4-pyridyl)propane) have been successfully prepared and characterized (Scheme 1). The coordination modes of the ligands are discussed in detail herein, and, in addition, the thermal stabilities and hydrogen adsorption properties of **3** and **4** are also presented.

Experimental Section

General Procedures. All chemicals for synthesis were obtained from commercial sources and used without further purification, with the exception of 1,4-bis(4-pyridyl)-2,3-diaza-1,3-butadiene (bpdab), prepared according to the literature procedure.[24] Elemental analyses of C, H, and N were performed by the Elemental Analysis Service of the School of Chemistry, University of Nottingham. Infrared spectra were measured as KBr discs on a Nicolet Avatar 360 FT-IR system over the 400−4000 cm^{-1} range. Thermal gravimetric (TG) measurements were performed on a Rheometric Scientific STA 1500H thermal analyzer at a heating rate of 1 °C/min^{-1} under nitrogen flow (generally 60 mL/min). X-ray powder diffraction data were collected on a Philips X'pert powder diffractometer with Cu K_α radiation from samples mounted on the flat glass plate sample holder. Scans of approximately 90 min were run for each sample over the range $5° \le 2\theta \le 60°$ with a step size of 0.02° in 2θ. Simulated powder patterns were generated from CIF data for the final single crystal refinement model using MERCURY.[25]

Synthesis of $[Zn_2(hfipbb)_2(py)_2]\cdot DMF$ (1). A mixture of $Zn(NO_3)\cdot 6H_2O$ (29.7 mg, 0.10 mmol), H_2hfipbb (39.2 mg, 0.10 mmol), and pyridine (0.1 mL) was dissolved in *N*,*N*-dimethylformamide (DMF; 8 mL), sealed in a 23 mL Parr

(23) (a) Monge, A.; Snejko, N.; Gutiérrez-Puebla, E.; Medina, M.; Cascales, C.; Ruiz-Valero, C.; Iglesias, M.; Gómez-Lor, B. *Chem. Commun.* **2005**, 1291. (b) Gándara, F.; de Andrés, A.; Gómez-Lor, B.; Gutiérrez-Puebla, E.; Iglesias, M.; Monge, M. A.; Proserpio, D. M.; Snejko, N. *Cryst. Growth Des.* **2008**, *8*, 378. (c) Zhou, Y.; Han, L; Pan, J.; Li, X.; Zheng, Y. *Inorg. Chem. Commun.* **2008**, *11*, 1107. (d) Harbuzaru, B. V.; Corma, A.; Rey, F.; Atienzar, P.; Jordá, J. L.; García, H.; Ananias, D.; Carlos, L. D.; Rocha, J. *Angew. Chem., Int. Ed.* **2008**, *47*, 1080. (e) Gándara, F.; Gomez-Lor, B.; Gutiérrez-Puebla, E.; Iglesias, M.; Monge, M. A.; Proserpio, D. M.; Snejko, N. *Chem. Mater.* **2008**, *20*, 72. (f) Leea, J.; Li, J.; Jagiello, J. *J. Solid State Chem.* **2005**, *178*, 2527. (g) Liu, Z.; Stern, C. L.; Lambert, J. B. *Organometallics* **2009**, *28*, 84.

(24) Dong, Y. B.; Zhao, X.; Huang, R.; Smith, M. D.; zur Loye, H. C. *Inorg. Chem.* **2004**, *43*, 5603.

(25) (a) Nolze, G.; Kraus, W. *Powder Diffr.* **1998**, *13*, 256. (b) *MERCURY*, version 1.4.2; http://www.ccdc.cam.ac.uk/products/mercury.

bomb, and heated at 120 °C for 3 days. This afforded colorless crystals of **1**, which were collected by filtration, washed with ethanol, and dried in air. Yield 37.8 mg (66.2%). Elemental analysis for $C_{47}H_{33}F_{12}N_3O_9Zn_2$ (calcd/found): C, 49.58/49.56; H, 2.92/2.91; N, 3.69/3.71. Selected IR(KBr, ν_{max}): 1659 (s), 1601(s), 1528(m), 1384(m), 1212(m), 966(m) cm^{-1}.

Synthesis of $[Zn_2(hfipbb)_2(bpy)(H_2O)]$ (2). A mixture of $Zn(NO_3)\cdot 6H_2O$ (15.8 mg, 0.054 mmol), H_2hfipbb (21 mg, 0.054 mmol), and 4,4′-bipy (15.6 mg, 0.10 mmol) was suspended in H_2O (9 mL), sealed in a 23 mL Parr bomb, and heated at 125 °C for 4 days. This afforded colorless crystals of **2**, which were collected by filtration, washed with ethanol, and dried in air. Yield 10.3 mg (35.7%). Elemental analysis for $C_{44}H_{26}F_{12}N_2O_9Zn_2$ (calcd/found): C, 48.87/48.91; H, 2.42/2.46; N, 2.59/2.61. Selected IR(KBr, ν_{max}): 3428(br), 1659(s), 1601(s), 1212(m), 966(m), 857(m), 782(m), 458 (w) cm^{-1}.

Synthesis of $[Zn_2(hfipbb)_2(bpdab)]\cdot 2DMF$ (3). A mixture of $Zn(NO_3)\cdot 6H_2O$ (18.0 mg, 0.061 mmol), H_2hfipbb (25.3 mg, 0.065 mmol), and 1,4-bis(4-pyridyl)-2,3-diaza-1,3-butadiene (bpdab, 10.5 mg, 0.050 mmol) was suspended in DMF (20 mL), sealed in a 25 mL reaction tube, and heated in an oil bath at 100 °C for 60 h. This afforded yellow crystals of **3**, which were collected by filtration, washed with methanol, and dried in air. Yield 24.5 mg (60.3%). Elemental analysis for $C_{55}H_{47}F_{12}N_7O_{11}Zn_2$ (calcd/found): C, 49.42/49.39; H, 3.54/3.53; N, 7.33/7.31. Selected IR(KBr, ν_{max}): 3075(s), 1685(m), 1635(s), 1563(s), 1399(m), 1214(m), 962(m), 841(m) cm^{-1}.

Synthesis of $[Cd_2(hfipbb)_2(DMF)_2]\cdot 2DMF$ (4). $Cd(NO_3)_2\cdot 6H_2O$ (19.6 mg. 0.06 mmol), H_2hfipbb (20.8 mg, 0.05 mmol), and 4,4′-bipyridine (4,4′-bipy, 7.8 mg, 0.050 mmol) were mixed and stirred in DMF (9 mL) for several minutes, sealed in a 25 mL reaction tube, and heated in an oil bath at 100 °C for 3 days. This afforded colorless crystals of **4**, which were collected by filtration, washed with DMF and ethanol, and dried in air. Yield 25.7 mg (65.5%). Elemental analysis for $C_{46}H_{44}Cd_2F_{12}N_4O_{12}$ (calcd/found): C, 42.58/42.60; H, 3.42/3.46; N, 4.32/4.38; Selected IR(KBr, ν_{max}): 2986(s), 1659(s), 1602(s) cm^{-1}.

Synthesis of $[Co(hfipbb)(dpp)]\cdot MeOH$ (5). A mixture of $Co(NO_3)\cdot 6H_2O$ (15.7 mg, 0.054 mmol), H_2hfipbb (21.8 mg, 0.056 mmol), and 1,3-di(4-pyridyl)propane (dpp, 21 mg, 0.106 mmol) was suspended in H_2O (4 mL) and MeOH (4 mL), sealed in a 23 mL Parr bomb, and heated at 130 °C for 4 days. This afforded purple crystals of **5**, which were collected by filtration, washed with methanol and dried in air. Yield 14.8 mg (40.4%). Elemental analysis for $C_{31}H_{26}CoF_6N_2O_5$ (calcd/found): C, 54.80/54.77; H, 3.86/3.84; N, 4.12/4.17. Selected IR (KBr, ν_{max}): 3468(br), 3079(s), 1654(s), 1597(s), 1210(m), 746(m) cm^{-1}.

X-ray Crystallography. Suitable crystals were glued to glass fibers and mounted on a Bruker SMART APEX CCD area detector diffractometer equipped with an Oxford Cryosystems open-flow cryostat and graphite monochromated Mo Kα radiation ($\lambda = 0.71073$ Å). Data were collected at 150 K, reduced and corrected for Lorentz and polarization effects using the SAINT[26] program and for absorption using the SADABS[27] program. The structures were solved by direct methods using SHELXS[28] and refined with the full-matrix least-squares technique using SHELXTL.[28] The non-H atoms, with the exception of those in disordered solvent molecules, were modeled with anisotropic displacement parameters, and refined by the full-matrix least-squares on F^2. Carbon-bound H atoms were placed in calculated positions and refined using the riding model. In the structures of **2** and **5** the starting positions for water (**2**) and methanol (**5**) H atoms were located from the difference Fourier syntheses, and then refined either with restraints for O−H bonds of coordinated water molecules or by using a geometrical model for methanol molecules. Further details for crystallographic data and refinement conditions are summarized in Table 1, and selected bond lengths and bond angles are given in Supporting Information, Table S1.

Hydrogen Adsorption Measurements. Hydrogen adsorption−desorption experiments were conducted at 77 K using an IGA gravimetric adsorption apparatus equipped with a microgram balance, 2 mbar, 100 mbar, and 20 bar pressure transducers, and a clean ultrahigh vacuum system. Ultrapure H_2 (99.9995%) was purified further by using calcium aluminosilicate adsorbents to remove trace amounts of water and other impurities before introduction into the IGA system. For measurements at 77 K, a standard low-temperature liquid nitrogen Dewar vessel was used. Before gas adsorption measurements, the sample was activated at 150 °C (for **3**) and 200 °C (for **4**) under ultrahigh vacuum (10^{-8} mbar) overnight. About 50 mg of samples were loaded for gas adsorption, and the weight of each sample was recorded before and after outgassing to confirm complete removal of all guest molecules including the coordinated DMF in **4**. All isotherm data points were fitted by the IGASwin system software v.1.03.143 (Hiden Isochema, 2004) using a linear driving force model when >98% equilibration had been reached. All changes in sample weight were corrected for buoyancy effects.

Results and Discussion

Synthesis. Hydro(solvo)thermal synthetic methods were used for the synthesis and crystallization of metal complexes. An interesting 2-fold parallel interpenetrated layered network $[Zn_2(hfipbb)_2(py)_2]\cdot DMF$ (**1**) was obtained by heating H_2hfipbb, $Zn(NO_3)_2\cdot 6H_2O$ and pyridine in DMF at 120 °C. The coordinated pyridine molecules in **1** are nearly perpendicular to the layers and protrude into the interlamellar regions. This suggests that the coordinated pyridine molecules in **1** might be replaced by neutral bridging *N,N′*-donors to form pillared frameworks with potential stable porosity. The solvothermal reaction of H_2hfipbb and $Zn(NO_3)_2\cdot 6H_2O$ in the presence of 4,4′-bipy, however, afforded an alternative layered coordination framework, $[Zn_2(hfipbb)_2(4,4'\text{-bipy})(H_2O)]$ (**2**). When the spacer of the auxiliary ligands is elongated to 1,4-bis(4-pyridyl)-2,3-diaza-1,3-butadiene (bpdab), the corresponding solvothermal reactions of $Zn(NO_3)_2\cdot 6H_2O$ with H_2hfipbb gave the targeted 3D 2-fold interpenetrated framework, $[Zn_2(hfipbb)_2(bpdab)]\cdot 2DMF$ (**3**), the structure of which is composed of layers of $\{Zn_2\}$ paddlewheels and bpdab pillars. The solvothermal reaction of H_2hfipbb, $Cd(NO_3)_2\cdot 6H_2O$ and 4,4′-bipy in DMF afforded a unique layered framework composed of helical tubes, $[Cd_2(hfipbb)_2(DMF)_2]\cdot 2DMF$ (**4**), that surprisingly does not include 4,4′bipy in the product. With 1,3-di(4-pyridyl)propane (dpp), the corresponding solvothermal reaction of H_2hfipbb with $Co(NO_3)_2\cdot 6H_2O$ in H_2O-MeOH mixture afforded $[Co(hfipbb)(dpp)]\cdot MeOH$ (**5**), a layered compound, structurally different from **1**−**4**.

Description of Crystal Structures

Structure of $[Zn_2(hfipbb)_2(py)_2]\cdot DMF$ (1). Single-crystal X-ray analysis revealed that **1** displays a 2-fold parallel 2D→2D interpenetrated polymeric structure with 1D helical channels. The asymmetric unit in **1** contains one

(26) *SAINT*, version 6.36a; Bruker AXS: Madison, WI, 2000.
(27) Sheldrick G. M. *SADABS*; University of Göttingen: Göttingen, Germany, 1996−2006.
(28) Sheldrick, G. M. *Acta Crystallogr., Sect. A* **2008**, *64*, 112.

Table 1. Crystallographic Data and Structure Refinement Summary for **1**–**5**

	1	**2**	**3**	**4**	**5**
chemical formula	$C_{47}H_{33}F_{12}N_3O_9Zn_2$	$C_{44}H_{26}F_{12}N_2O_9Zn_2$	$C_{55}H_{47}F_{12}N_7O_{11}Zn_2$	$C_{46}H_{44}Cd_2F_{12}N_4O_{12}$	$C_{31}H_{26}CoF_6N_2O_5$
fw	1142.50	1085.41	1340.74	1297.65	679.47
cryst size (mm^3)	0.44 × 0.35 × 0.12	0.44 × 0.19 × 0.07	0.37 × 0.20 × 0.02	0.45 × 0.20 × 0.09	0.57 × 0.19 × 0.05
space group	$C2/c$	$P2_1/c$	$Pca2_1$	$P2_1/c$	$P\bar{1}$
a (Å)	29.671(6)	26.240(3)	22.670(4)	11.983(2)	8.8564(12)
b (Å)	7.8424(16)	11.9953(13)	16.086(3)	15.990(2)	12.527(2)
c (Å)	23.240(5)	13.383(2)	15.833(3)	28.353(3)	14.169(2)
α (deg)	90	90	90	90	81.870(2)
β (deg)	121.070(3)	93.196(2)	90	104.736(5)	73.992(2)
γ (deg)	90	90	90	90	80.204(2)
V ($Å^3$)	4632(3)	4205.8(9)	5773.8(18)	5254(2)	1481.6(4)
ρ_{calcd} (g/cm^3)	1.638	1.714	1.542	1.641	1.523
θ_{min}, θ_{max} (deg)	2.02, 27.53	2.28, 27.54	2.02, 27.62	1.96, 27.56	2.12, 25.0
μ (mm^{-1})	1.144	1.255	0.935	0.914	0.661
F(000)	2304	2176	785	2592	694
no. of reflns	21317	18958	32111	47588	9268
no. of unique reflns	5686	9812	12923	12474	5069
no. of obsd reflns [$I > 2\sigma(I)$]	4723	5487	11875	10912	3624
no. of parameters	351	628	785	694	410
R_{int}	0.032	0.049	0.050	0.044	0.048
R^a, $R_w{}^b$	0.0321, 0.0900	0.0432, 0.0627	0.0740/0.151	0.0570, 0.131	0.0396, 0.0790
GOF[c]	1.13	0.982	1.199	1.109	0.993
residuals (e $Å^{-3}$)	0.45, −0.31	0.70, −0.64	0.71, −0.97	1.64, −1.99	0.45, −0.41

[a] $R = \sum||F_o| - |F_c||/\sum|F_o|$. [b] $R_w = [\sum w(F_o^2 - F_c^2)^2/\sum w(F_o^2)^2]^{1/2}$. [c] $GOF = \{\sum[w(F_o^2 - F_c^2)^2]/(n-p)\}^{1/2}$.

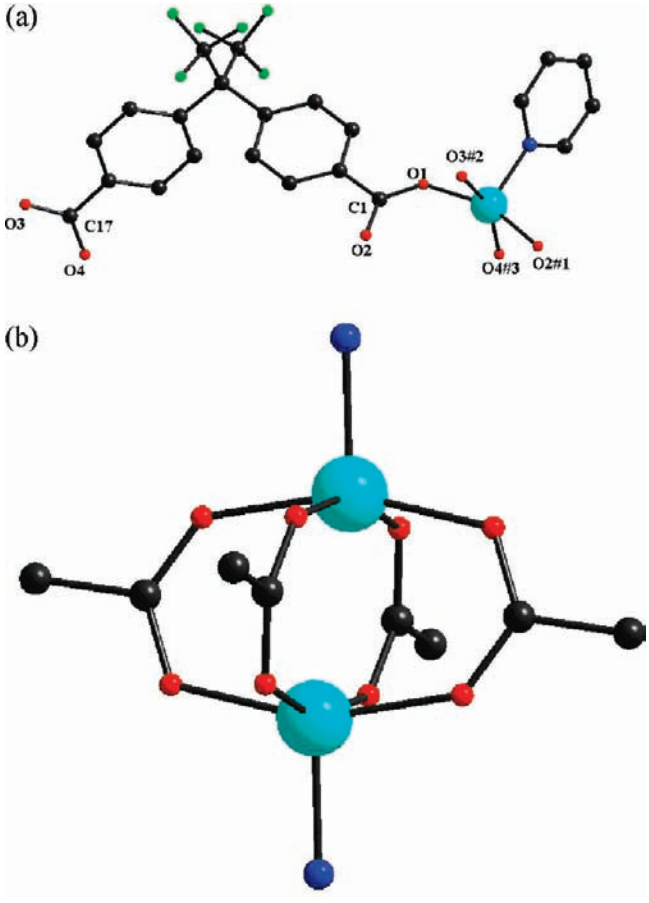

Figure 1. (a) Asymmetric unit of **1**, symmetry codes shown in Supporting Information, Table S1; (b) $\{Zn_2\}$ paddlewheel building unit observed for **1**.

Zn(II) ion, an $hfipbb^{2-}$ ligand, and one coordinated pyridine molecule and a guest DMF solvent molecule (Figure 1a) with the metal-based building unit comprising a binuclear Zn(II)-tetracarboxylate paddlewheel cluster. In this binuclear unit (Figure 1b), each Zn(II) ion resides in a square pyramidal coordination geometry with the apical position occupied by a coordinated pyridine molecule [Zn−N(apical) = 2.0300(15) Å], while the basal plane consists of four carboxylate O atoms [Zn−O = 2.0295(14)−2.0593(12) Å]. The intradimer Zn···Zn separation is 2.9758(7) Å, within the normal range found in other reported bimetallic paddlewheel units of type $[M_2(O_2CR)_4]$.[29] In **1**, each paddlewheel unit connects to four neighboring paddlewheel clusters via bridging $hfipbb^{2-}$ dianions, which adopt a bridging tetradentate mode (Scheme 2a) to form a 2D undulating (4,4) net with large rhomb-like windows (Figure 2a). The dimensions of the rhombic window are 14.02 × 14.02 $Å^2$ as measured between the centroids of the binuclear Zn(II) subunits at the corners of the window. As depicted in Figure 2b, the skeleton of this 2D sheet can also be described as a unique helical layer in which the left and right helical chains appear alternatively by sharing the paddlewheel clusters. The pitch of helix is double the b parameter (15.685 Å).

Most strikingly, the two diagonals of the rhombic window are equal to unit cell parameters b and c, respectively. Two closest identical helical layers shift by b so that the paddlewheel units from one layer fall in the center of the window of the other layer, and interpenetrate each other in a parallel 2D→2D fashion, resulting in an interwoven bilayer with 1D double helical channels (Figures 2b and 2c). The $hfipbb^{2-}$ ligand

(29) (a) Eddaoudi, M.; Li, H.; Yaghi, O. M. *J. Am. Chem. Soc.* **2000**, *122*, 1391. (b) Eddaoudi, M.; Kim, J.; Wachter, J. B.; Chae, H. K.; O'Keeffe, M.; Yaghi, O. M. *J. Am. Chem. Soc.* **2001**, *123*, 4368. (c) Wang, R.; Han, L.; Jiang, F.; Zhou, Y.; Yuan, D.; Hong, M. *Cryst. Growth Des.* **2005**, *5*, 129. (d) Guo, X.; Zhu, G.; Fang, Q.; Xue, M.; Tian, G.; Sun, J.; Li, X.; Qiu, S. *Inorg. Chem.* **2005**, *44*, 3850. (e) Chui, S. S.-Y.; Lo, S. M.-F.; Charmant, J. P. H.; Orpen, A. G.; Williams, I. D. *Science* **1999**, *283*, 1148. (f) Vos, T. E.; Liao, Y.; Shum, W. W.; Her, J.-H.; Stephen, P. W.; Reiff, W. M.; Miller, J. S. *J. Am. Chem. Soc.* **2004**, *126*, 11630. (g) Han, L.; Zhou, Y.; Zhao, W.-N.; Li, X.; Liang, Y.-X. *Cryst. Growth Des.* **2009**, *9*, 660.

Scheme 2. Bridging Coordination Modes of $hfipbb^{2-}$ Ligands Observed[a]

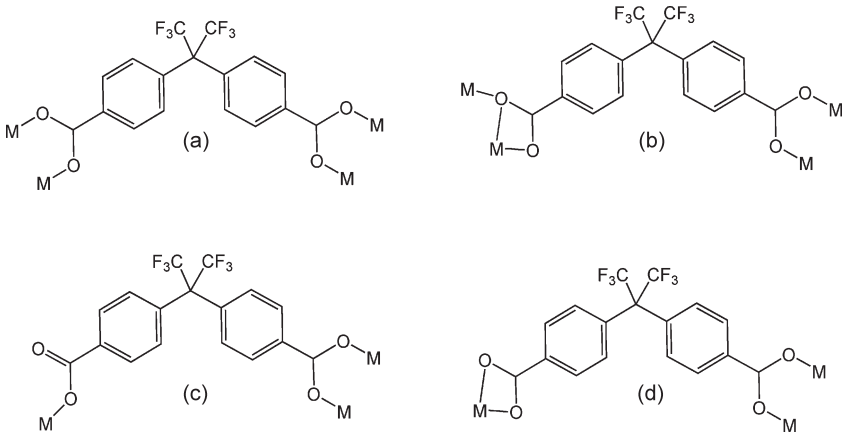

[a] (a) Bridging tetradentate mode observed in **1**, **3**, and **4**; (b) bridging chelated tetradentate mode observed in **4**; (c) bridging tridentate mode observed in **2**; (d) bridging chelated tridentate mode observed in **2** and **5**.

presents a dihedral angle of 72.7° between the two benzene rings, and this configuration contributes to the parallel 2D→2D interpenetration. Stacking of the interwoven bilayers along the *a*-axis reveals the coordinated pyridyl molecules lying almost perpendicular to the layers, but they are not long enough to create solvent-accessible interlamellar space. The effective void volume estimated by PLATON/SOLV[30] is only 575.9 Å^3 corresponding to 12.4% of the unit cell volume of 4632(3) Å^3. Disordered DMF molecules reside within the helical channels. There are also weak interlayer C−H···F hydrogen bonds formed between fluorine atoms and pyridine C−H groups at the edges of adjacent interwoven bilayers [H···F = 2.36−2.38 Å, C···F = 2.997(3)−3.005(2) Å]. A similar cobalt-hfipbb coordination polymer has been reported recently.[29g]

Structure of $[Zn_2(hfipbb)_2(bpy)(H_2O)]$ (2). To extend the parallel interpenetrating helical bilayers into 3D frameworks, we employed the rod-like exobisdentate 4,4′-bipy as a co-ligand to replace the monodendate pyridine molecule in **1**. However, the reaction of $Zn(NO_3)_2\cdot 6H_2O$, $H_2hfipbb$, and 4,4′-bipy did not afford the targeted 3D coordination polymer, but a different layered compound, $[Zn_2(hfipbb)_2(bpy)(H_2O)]$ (**2**). Single crystal X-ray diffraction reveals that **2** contains two distinct Zn(II) ions in the asymmetric unit (Figure 3a). Zn1 has a distorted octahedral coordination geometry, provided by four oxygens [Zn−O = 2.007(2)−2.317(2) Å] from three carboxylate ligands, one pyridyl nitrogen [Zn−N = 2.094(2) Å] and one water molecule [Zn−O = 2.125(2) Å]. Zn2 is tetrahedrally coordinated by three carboxylate oxygen atoms [Zn−O = 1.934(2)−1.965(2) Å] and one pyridyl nitrogen [Zn−N = 2.038(2) Å]. The two Zn(II) centers are bridged by a pair of *syn-syn* $hfipbb^{2-}$ carboxylate groups into a binuclear unit with intradimer Zn···Zn separation of 3.891 Å. Significantly, these binuclear units are doubly interlinked by the bent $hfipbb^{2-}$ moieties to form an infinite ribbon where two different bridging modes of the $hfipbb^{2-}$ ligands can be distinguished (Scheme 2c and d).

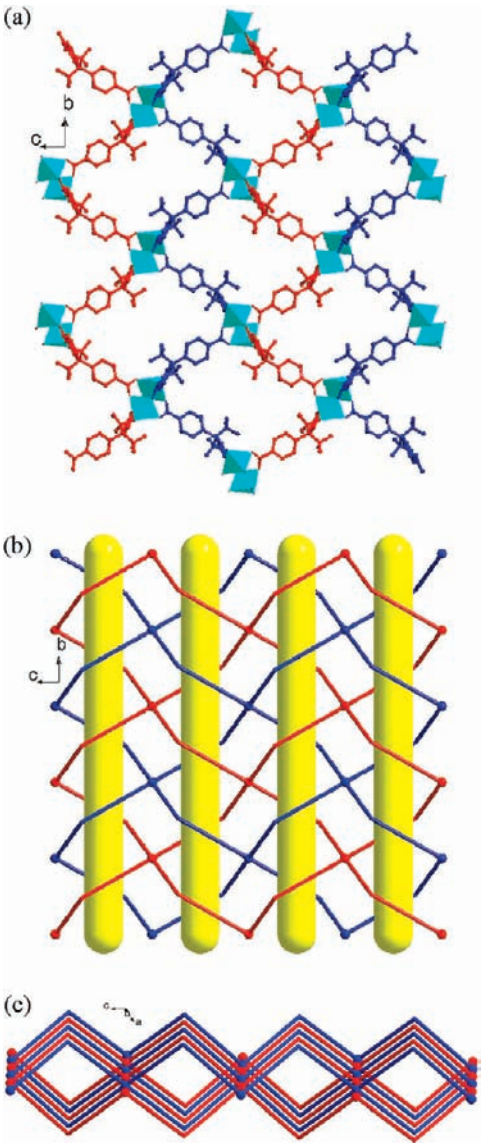

Figure 2. (a) Undulating layers in **1** with (4,4) topology. (b) and (c) schematic representations of 2-fold parallel 2D→2D interpenetration in **1** with 1D double helical channels (viewed along the *a* axis and close to the [010] direction, respectively).

(30) (a) Spek, A. L. *J. Appl. Crystallogr.* **2003**, 7. (b) Sluis, P.v.d.; Spek, A. L. *Acta Crystallogr., Sect. A* **1990**, *46*, 194.

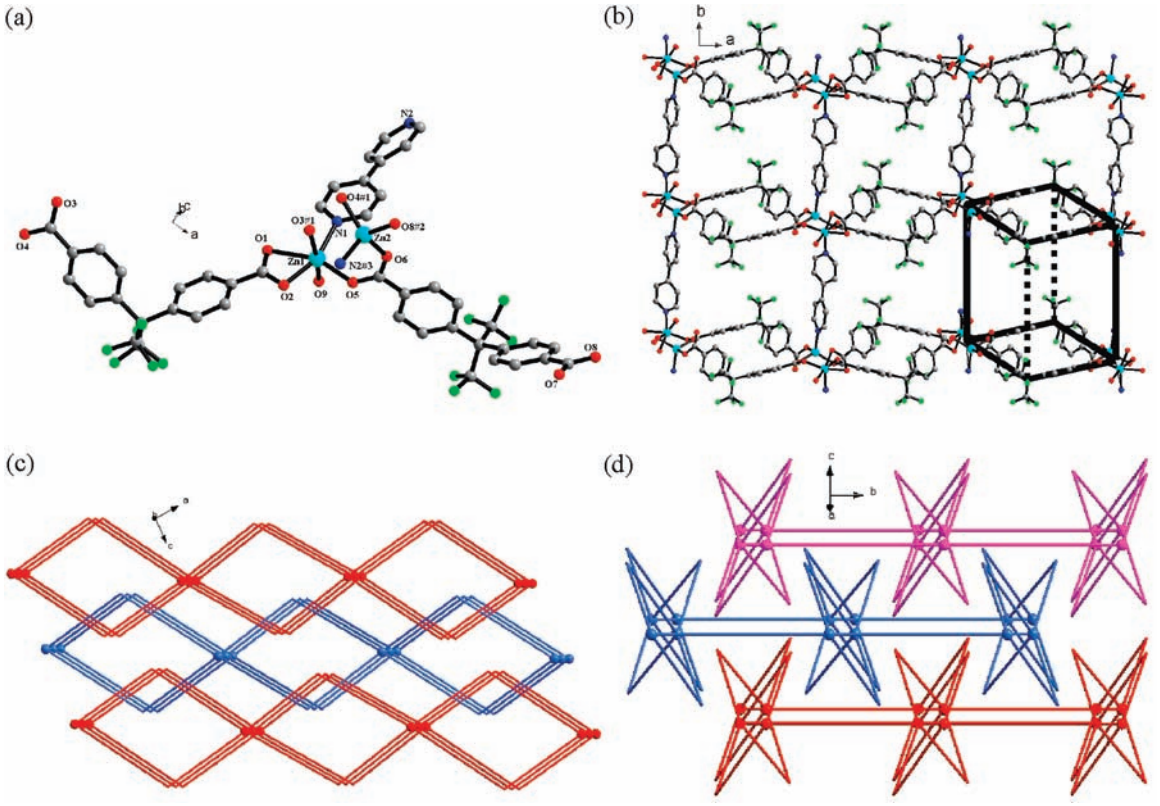

Figure 3. (a) View of the metal coordination environment in **2**. Guest solvent molecules and hydrogen atoms have been omitted for clarity; symmetry codes are given in Supporting Information, Table S1. (b) 2D infinite networks with large quasi-cuboid cavities within the lamella (viewed along the [001] direction). A schematic representation of the quasi-cuboid cavities is also highlighted (C, dark gray, O, red, N, blue, F, green, Zn, cyan). Hydrogen atoms have been omitted for clarity. (c) and (d) Schematic representations of interdigitation between layers in **2** (viewed close to the [010] direction).

The infinite ribbons formed by Zn(II) ions and $hfipbb^{2-}$ ligands in **2** are further connected through 4,4′-bipy ligands within a 2D network. If the central carbon atom linked to two CF_3 groups and two benzene spacers of each $hfipbb^{2-}$ ligand is considered as one of four corners of a cuboid and the Zn(II) binuclear units occupy the other four corner sites of the cuboid, then large quasi-cuboid cavities can be envisaged (Figure 3b). However, these layers are tightly stacked in an ···ABAB··· fashion along the crystallographic *c* axis. Furthermore, CF_3 groups from adjacent layers are embedded into the quasi-cuboid cavities of a layer at both sides of the layer, resulting in no overall porosity for **2** (Figure 3c and 3d). The PLATON/SOLV[30] calculation shows no effective void volume (only 0.7% of the unit cell volume), and hydrogen bonds between layers further lead to a tightly packed structure O_w-H···$O_{carboxylate}$ [H···O = 1.828(11)−2.241(16) Å, O··O = 2.668(3)−3.014(3) Å] and weak C−H···F [H···F = 2.46 Å, C···F = 3.405(4) Å] or C−H···$O_{carboxylate}$ [H···O = 2.54 Å, C···O = 3.468(4) Å].

Structure of $[Zn_2(hfipbb)_2(bpdab)]\cdot 2DMF$ (3). Complex **3** crystallizes in the orthorhombic space group $Pca2_1$, and the Zn(II) local coordination geometry is similar to that in **1** with pairs of Zn(II) centers forming a binuclear Zn(II)-tetracarboxylate paddlewheel cluster node (cf., Figure 1b). These are bridged by $hfipbb^{2-}$ ligands into a (4,4) helical layer with large rhombic pores, and in contrast to **1**, the two axial sites of each paddlewheel unit in **3** are occupied by N-donors from bpdab pillars (Figure 4a). As expected, the helical layer is identical to that of **1**, and two identical helical layers are interpenetrated in a parallel 2D→2D fashion. Upon 2-fold parallel interpenetration, 1D double helical channels (**A**) in the skeleton are formed (Supporting Information, Figure S3b). However in **3**, adjacent layers are pillared by 1,4-bis(4-pyridyl)-2,3-diaza-1,3-butadiene (bpdab) ligands to generate a 3D network (Figure 4b) of α-Po topology with additional interlamellar 1D channels (**B**) (Figure 4c). Thus the interpenetrating helical layers have been successfully extended by pillars to form targeted 3D frameworks with the effective void volume[30] drastically increasing from 12.4% (for **1**) to 30.8% (for **3**) of the crystal volume. Disordered DMF molecules in the channels **A** and **B** (Figure 4c) are anchored to the host framework via weak C−H···O_{DMF} hydrogen bonds (H···O = 2.30−2.52 Å, C···O = 3.215(11)−3.370(10) Å, and <CHO = 162−170°).

Structure of $[Cd_2(hfipbb)_2(DMF)_2]\cdot 2DMF$ (4). Complex **4** crystallizes in monoclinic space group $P2_1/c$, and the asymmetric unit consists of two Cd(II) ions, two $hfipbb^{2-}$ dianions, two coordinated DMF molecules, and two lattice DMF molecules (Figure 5a). The two crystallographically independent Cd(II) centers have different coordination geometries: Cd1 is coordinated by five carboxylate oxygens from four $hfipbb^{2-}$ ligands forming a distorted square pyramid, while the Cd2 center is octahedrally coordinated by four carboxylate oxygens in the equatorial plane [Cd−O = 2.193(4)−2.533(3) Å] and by the O-donors from two DMF

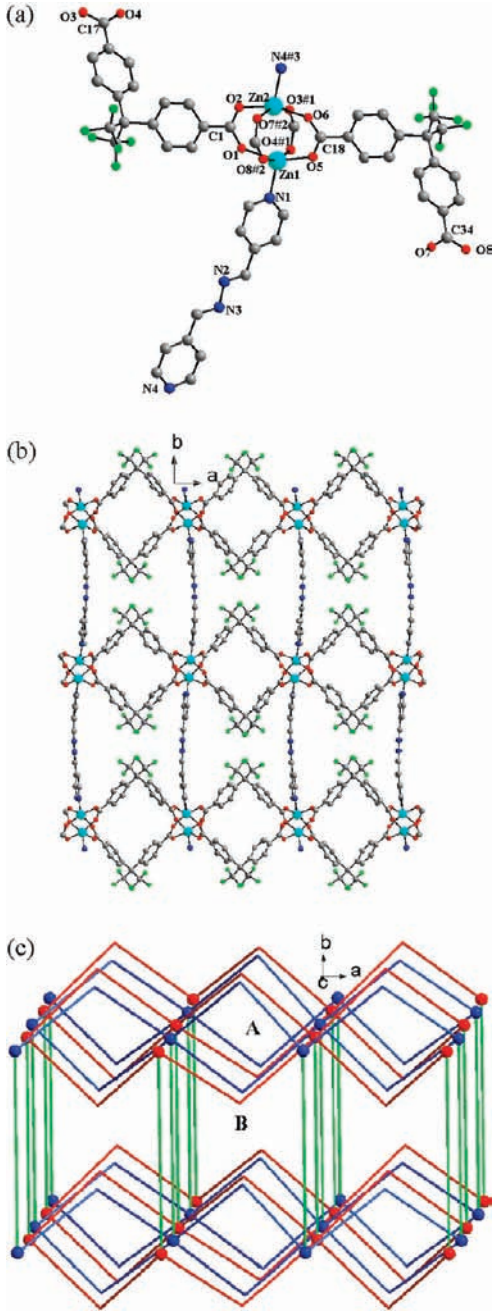

Figure 4. (a) View of the metal coordination environment in **3**. Guest solvent molecules and hydrogen atoms have been omitted for clarity. (b) The 3D pillar-layered framework in **3** (viewed along the *c* axis). (c) Schematic representation of the 2-fold interpenetrating network in **3** (the parallel interpenetrated helical layers are colored with red and blue, respectively, and pillars are shown as green lines).

molecules [Cd−O_{apical} = 2.252(4)−2.275(4) Å] in the axial positions. In **4**, the hfipbb^{2-} ligands present two different coordination modes: bridging tetradentate and bridging chelated tetradentate (Scheme 2a and 2b, respectively). Consequently, the Cd1···Cd2 pair is connected through two carboxylate groups to form corner-sharing binuclear building blocks, which are interlinked via μ_2-mode carboxylate groups to form a $[Cd_2(CO_2)_4]_n$ chain (Figure 5b). Linkages between chains via (hexafluoroisopropylidene)bis(benzene) spacers afford layers parallel to the crystallographic *ab* plane. Because of the geometry of hfipbb^{2-} ligands, double helical

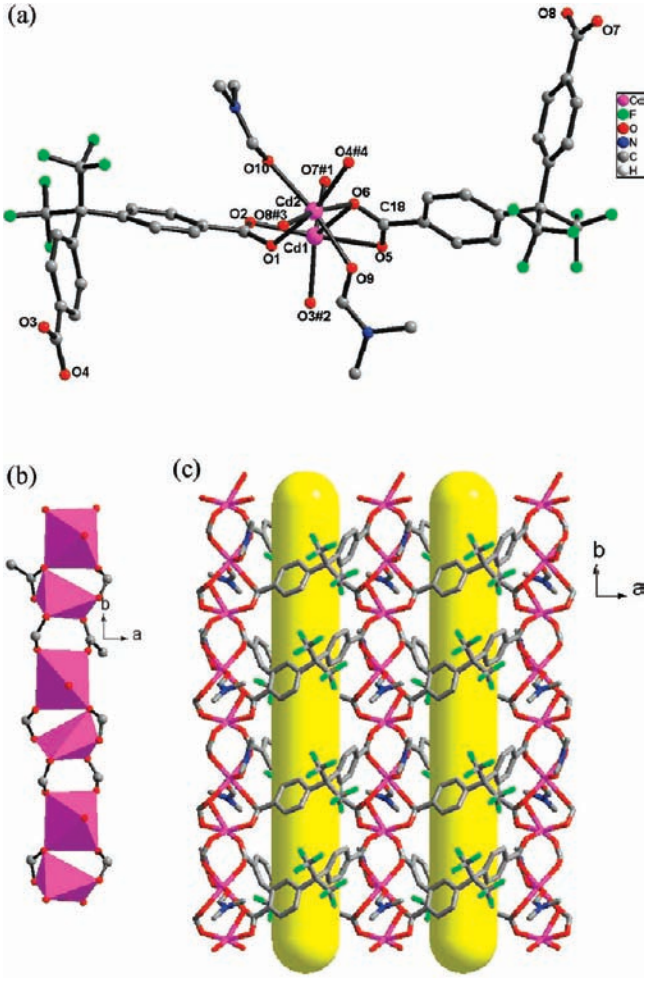

Figure 5. (a) Molecular structure of **4** showing the local coordination geometry at Cd(II) ions. Guest solvent molecules and hydrogen atoms have been omitted for clarity. Symmetry codes are given in Supporting Information, Table S1. (b) A view of the carboxylate-bridged $[Cd_2(CO_2)_4]_n$ chain formed by binuclear units via μ_2-mode carboxylate groups. (c) View of the layered structure of **4** with 1D double helical tubular channels.

tubular channels running along the *b* axis are formed within the layer with CF_3 groups on their periphery (Figure 5c), with accessible windows that can accommodate a sphere of diameter ~5.2 Å. The 1D intralamellar channels of **4** are similar to those found in the In(III) material [In(OH)(hfipbb)]·0.5py, which consists of $\{In(OH)\}_n$ chains linked together by hfipbb^{2-} ligands.[23e]

The double helical tubular channels inside each layer can alternatively be described as follows. Two crystallographically independent hfipbb^{2-} ligands (defined as L1 and L2, respectively, in Figure 6) are used to construct right-handed helical chains via coordination bonds between five-coordinated Cd(II) centers (Cd1) and L1 or L2. As shown in Figure 6a, two helical chains are intertwined with a period equal to the unit cell parameter *b* [15.990(2) Å] to form a double-stranded helical tube running along a 2_1 screw axis. The tubes are further aligned by sharing five-coordinated Cd1 centers to form a layered network with small pores. Each pore is defined by four carboxylate oxygen atoms from four hfipbb^{2-} ligands (Figure 6, panels b and c), and binds Cd2, which has an octahedral coordination geometry completed

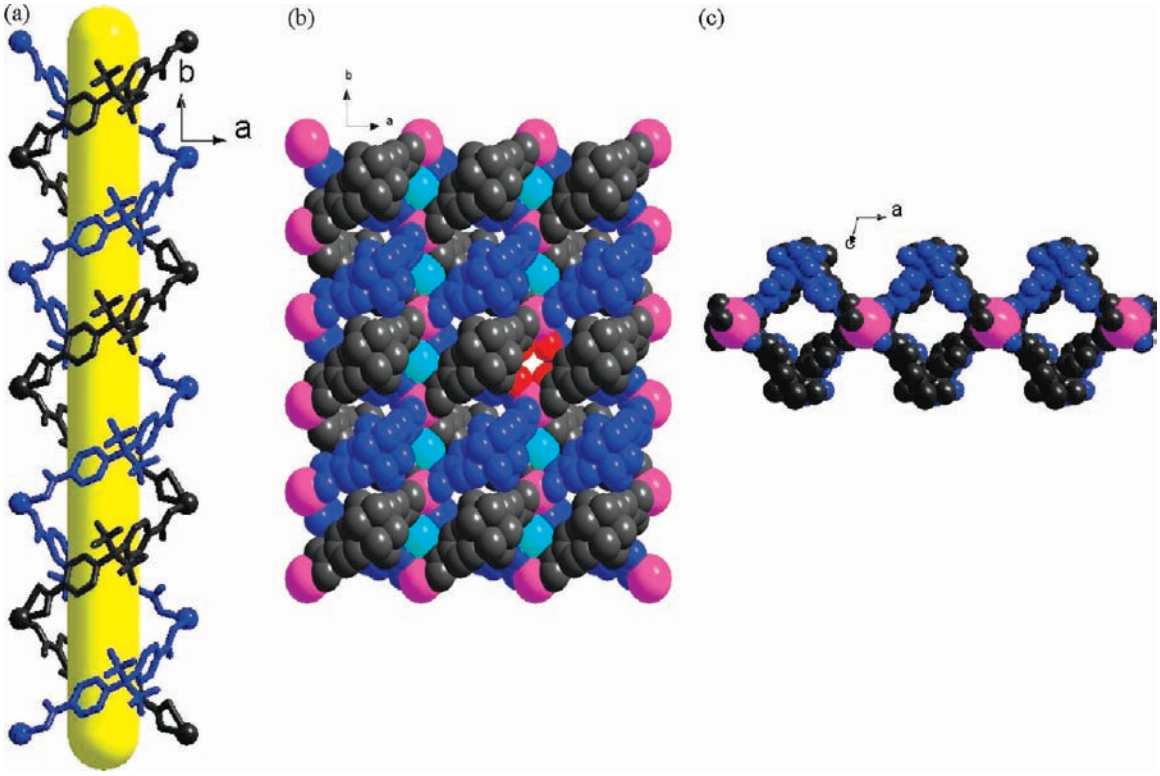

Figure 6. Views of the structure of **4**. (a) A side view of the double helical tube. Two intertwined right-handed helical chains are shown in different colors: black for the chain formed by Cd1 and L1, and blue for the chain formed by Cd1 and L2. (b) A space-filling view of the assembly of helical tubes into a 2D layered network with small pores each capturing octahedral Cd(II) ions (color modes: five-coordinated Cd1 atoms, purple; octahedral Cd2 centers, cyan; L1 ligands, black; L2 ligands, blue; and one pore highlighted in red). (c) View of 1D tubular channels within each layer. All hydrogen atoms and coordinated DMF molecules have been omitted for clarity.

by two axial oxygen atoms of two DMF molecules. The coordinated DMF molecules are nearly perpendicular to the layers, pointing into the interlamellar regions, revealing that the orientation of DMF is similar to that of the coordinated pyridine molecules in **1**. However, DMF molecules are smaller and more flexible than pyridine molecules and thus additional voids are created between the undulating layers. A PLATON/SOLV[30] calculation gives a value of 26.8% for the void space in the unit cell, and slightly more than half of this space is attributed to the 1D intralamellar tubular channels. Disordered DMF molecules situated in the intralamellar and interlamellar voids are bound to the host framework via weak $C_{aromatic}-H\cdots O_{DMF}$ or $C_{DMF}-H\cdots O_{carboxylate}$ hydrogen bonds ($C\cdots O$ = 3.12−3.41 Å; <CHO = 137−157°).

Structure of [Co(hfipbb)(dpp)]·MeOH (5). Single-crystal X-ray analysis reveals that the Co(II) ion in **5** has a slightly distorted octahedral coordination geometry, provided by three $hfipbb^{2-}$ and two dpp ligands [Co−O = 2.0325(18)−2.1828(19) Å; Co−N = 2.122(2)−2.165(2) Å]. As shown in Figure 7b, each pair of Co(II) ions is bridged by a pair of *syn-syn* $hfipbb^{2-}$ carboxylate groups to form a binuclear subunit, and these are doubly interlinked by the $hfipbb^{2-}$ ligands into an infinite ribbon, which is similar to that observed for **2**. However, only one coordination mode (Scheme 2d) is observed for the $hfipbb^{2-}$ ligands in **5**. In principle, dpp ligands can exhibit two conformations, *trans*−*trans* (TT) and *trans*−*gauche* (TG), with respect to the relative orientations of CH_2 groups.[29g] The two pyridyl nitrogens coordinated to each Co(II) ion in **5** are in *syn* positions [<N1−Co1−N2#3 = 92.74(8)°, #3 = $(x, 1 + y, z)$], and consequently, the dpp ligands in **5** only adopt the *trans-trans* (TT) conformation, and serve as double-bridges connecting $[Zn(hfipbb)]_n$ ribbons into a 2D (4,4) non-interpenetrating layer with two kinds of windows when viewed along the crystallographic *a* axis (Figure 7c). Window **A** is made up of two binuclear subunits and two $hfipbb^{2-}$ ligands along the ribbon (shortest diagonal $Zn\cdots Zn$ distance = 12.49 Å), while window **B** consists of two binuclear subunits and two dpp ligands perpendicular to ribbon chains (shortest diagonal $Zn\cdots Zn$ distance = 10.26 Å). These layers stack in such a way that lattice methanol molecules are anchored on either side of window **B** via strong $O_{methanol}-H\cdots O$ hydrogen bonds [$H\cdots O$ = 1.89 Å, $O\cdots O$ = 2.767(3) Å and <OHO = 172°].

Structural Discussion. We have synthesized five coordination polymers **1**−**5**, as illustrated in Scheme 1, that form 2D or 3D frameworks with diverse architectures. In complexes **1**−**5**, pairs of metal ions are bridged by carboxylate groups to form bimetallic clusters nodes which play an important role in determining the resulting network structure. A total of four different coordination modes of carboxylate groups are observed in **1**−**5** (Scheme 3). In the $\mu_2{}^b$-OCO coordination mode, both carboxylate oxygen atoms are involved in coordination to two M(II) atoms in a monodentate fashion; in the second coordination mode ($\mu_1{}^c$-OCO), both oxygen atoms of the carboxylate group are involved, but in this case only coordinated to one metal atom in an asymmetric chelating bidentate manner; in the third

Scheme 3. Summary of Coordination Modes of Carboxylate Groups Observed in **1**−**5**

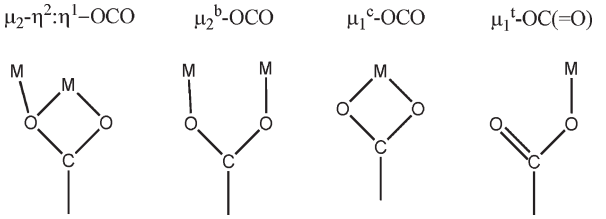

coordination mode (μ_2-η^2:η^1-OCO) the carboxylate group is coordinated to two metal sites in either monodentate to one metal or asymmetric chelating bidentate fashion to the other metal; the final coordination mode that is observed is the $\mu_1{}^t$-O(C═O), which has only one carboxylate oxygen coordinated to a metal center. The combination of the hfipbb^{2-} spacer and these carboxylate coordination modes can produce 10 possible bridging modes of hfipbb^{2-} ligands (Supporting Information, Scheme S1),[6f,23,29g] four of which are observed in compounds **1**−**5**. The bridging tetradentate mode of hfipbb^{2-} (Scheme 2a) results in the formation of bimetallic tetracarboxylate paddlewheel clusters, as shown in **1** and **3** and other previously reported compounds.,[6f,23g,23f,29g] where the apical positions of the paddlewheel units can be either occupied by terminal ligands (e.g., py in **1** and in [Co(hfipbb)(py)][29g]) or neutral bridging pillars (e.g., bpdab in **3** and H_2hfipbb in ([Cu(hfipbb)(H_2hfipbb)$_{0.5}$][6f]). The hfipbb^{2-} ligands in **2** exhibit two different bridging modes (Scheme 2c and 2d) and link binuclear Zn(II) units to form [Zn(hfipbb)]$_n$ ribbon-like chains, while the py moieties of 4,4′-bipy are coordinated to the Zn-carboxylate units in a *trans* fashion, resulting in a (4,4) network based on a binuclear cluster node, double-stranded hfipbb^{2-} linkers and single-stranded 4,4′-bipy linkers. Although **5** contains a similar ribbon-like chain to that of **2**, the hfipbb^{2-} ligands in **5** only take the bridging chelated tridentate mode (Scheme 2d), and, thus, the py moieties of dpp occupy two *cis* positions to fulfill the pseudo-octahedral coordination at each Co(II) center. The resultant structure is a non-interpenetrated (4,4) network based on binuclear cluster nodes and double-stranded organic linkers (Figure 7c). The Cd(II) complex **4** is the only compound described here where two distinct bridging modes of hfipbb^{2-} are exploited to generate the layer structure, with no additional bipyridyl spacers used. Thus, Cd(II) centers with different coordination geometries are linked by both μ_2-η^2:η^1-OCO and $\mu_2{}^b$-OCO groups into [$Cd_2(O_2C)_4$]$_n$ chains that are further linked via hfipbb^{2-} spacers to form a 2D network with tubular helical channels inside the layer.

Thermal Stability, XRD Analysis, and H_2 Adsorption. Because of the very low porosity of **1**, **2**, and **5**, as confirmed by single-crystal diffraction analysis, only **3** and **4** were studied for porosity and gas adsorption. Thermo gravimetric analysis (TGA) of **3** and **4** were studied under N_2 flow (60 mL/min) at a heating rate of 1 °C min^{-1}. As shown in Figure 8a (curve I), all the DMF in **3** is removed (weight loss, 16.4%, calcd 16.3%) by 250 °C. The desolvated form **3a** is stable up to ∼360 °C and then decomposes to an unidentified product. The thermal stability of **4** is similar, with the weight loss of

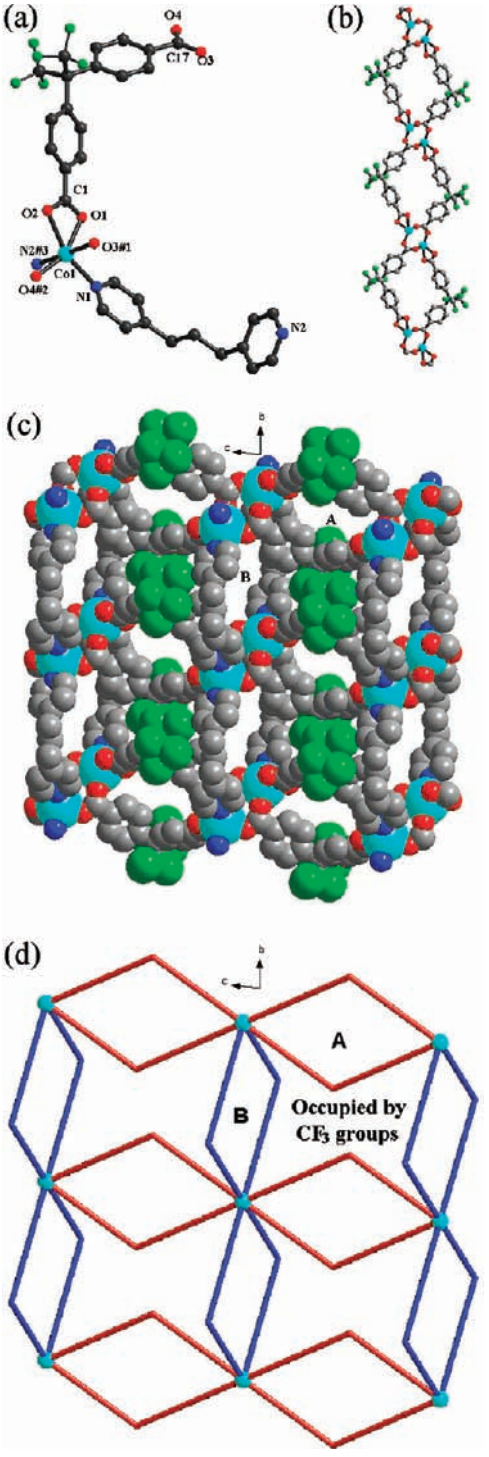

Figure 7. (a) View of the metal coordination environment in **5**. Symmetry codes are given in Supporting Information, Table S1. Guest solvent molecules and hydrogen atoms have been omitted for clarity. (b) View of the infinite ribbon-like chain made up of binuclear Co(II) nodes. (c) Space-filling representation of the 2D layer in **5**. (d) Schematic representation of the (4,4) network of **5** based on double-stranded organic linkers (bent hfipbb^{2-} and dpp ligands presented as red and blue lines, respectively; the cyano-colored balls representing the center of binuclear cobalt subunits as 4-connected nodes).

20.3% completed at around 250 °C (curve IV in Figure 8a), corresponding to the loss of all the guest and coordinated DMF (calcd 22.5%). The weight loss beginning at ∼350 °C corresponds to the decomposition of the framework.

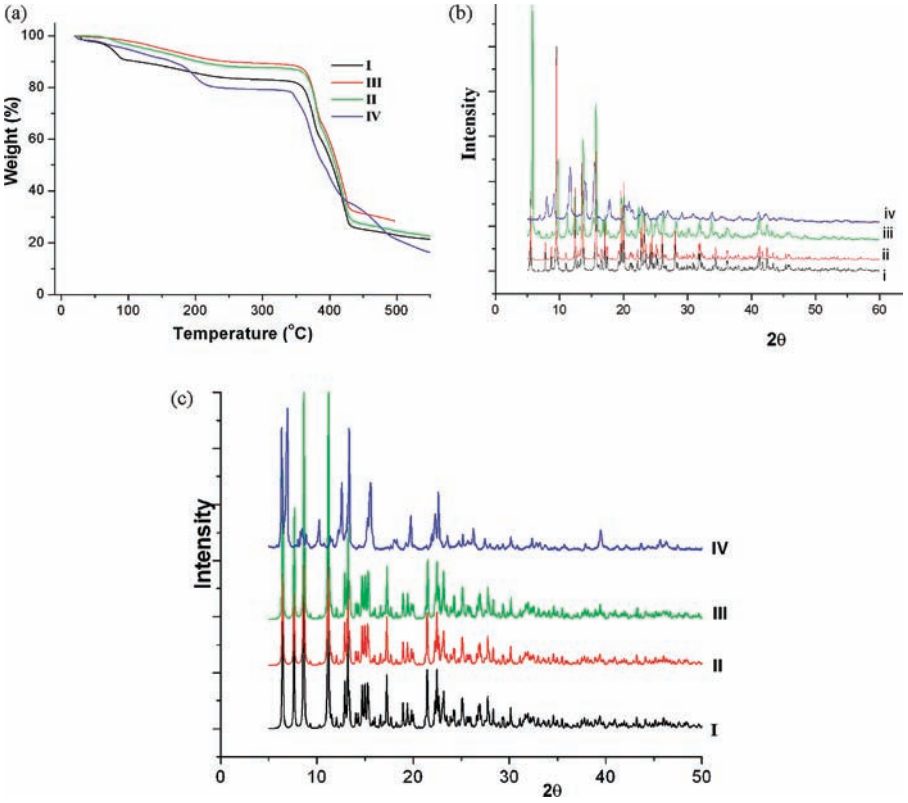

Figure 8. (a) TGA analysis of **3** and **4**. Curve I is that of the as-prepared sample of **3**. Curves II and III are for samples obtained by immersing the desolvated host crystals of **3a** in DMF for 6 h and 1 day, respectively. Curve IV represents the as-synthesized sample of **4**. (b) Powder XRD patterns of **3**. I simulated from single-crystal diffraction data, II for as-synthesized crystals, III for the sample **3a** after reintroducing DMF, IV for the sample (**3a**) prepared by heating **3** at 260 °C under N_2 flow for 6 h or by evacuating **3** at 150 °C under ultrahigh vacuum (10^{-8} mbar) for overnight. (c) Powder XRD patterns of **4**. (I simulated from single-crystal diffraction data, II for as-synthesized crystals, III for the partly desolvated phase at 125 °C, and IV for the fully desolvated solid (**4a**) generated by heating **4** at 250 °C under N_2 flow for 3 h or by evacuating **4** at 200 °C under ultrahigh vacuum (10^{-8} mbar) for 20 h).

The purity and thermal stability of **3** and desolvated **3a** were confirmed by powder X-ray diffraction (PXRD) analysis (Figure 8b). The PXRD patterns for the evacuated sample obtained by heating **3** at 260 °C under N_2 flow for 6 h to give **3a** is similar to that of the as-synthesized crystalline solid, suggesting that the guest-free phase of **3** remains intact on desolvation. After removal of DMF, the host crystals were soaked in DMF and again subjected to TGA. The results revealed the loss of DMF is completed at the same temperature (250 °C). However, the quantity of DMF in the channels is 6.9 or 5.2% less (see curves III and II in Figure 8a) following 6 or 24 h immersion in DMF, respectively, compared to the as-prepared crystals. This indicates a reversible but gradual process of reintroducing DMF into the framework pores.[19a] Although we could not determine the single crystal structure after the reintroduction of DMF, its PXRD pattern (see III in Figure 8b) is identical to that of the as-prepared crystals of **3** (pattern II in Figure 8b).

A sample of **4** was heated to 125 °C under vacuum for 3 h to remove lattice DMF molecules. The partly desolvated phase $[Cd_2(hfipbb)_2(DMF)_2]$ shows a similar PXRD pattern to the one simulated from single-crystal diffraction of **4** (Figure 8c). However, after removal of coordinated DMF at 250 °C, the PXRD pattern changes slightly with a systematic shift to higher 2θ (lower *d*-spacing) values indicating a compaction of the stacked layers in the structure. The PXRD patterns, however, retain sharp reflections and return to the original on reintroduction of DMF, indicating that the fully desolvated form remains crystalline and microporous (see below); such microporosity can be attributed to the retention microtubes inside the layers after desolvation.

To evaluate further the microporosity of these materials, the adsorption of N_2, CO_2, and H_2 were investigated for the desolvated (guest-free) forms of **3** and **4** (i.e., **3a** and **4a**, respectively). As shown in Figure 9a, the CO_2 adsorption of **3a** and **4a** at 195 K exhibits a reversible type-I isotherm characteristic of microporous material. The uptake of CO_2 for **3a** and **4a** at 1 bar corresponds to 2.67 mmol g^{-1} (or 60 cm^3 g^{-1}) and 1.83 mmol g^{-1} (or 41 cm^3 g^{-1}), respectively, and the Brunauer−Emmett−Teller (BET; Langmuir) surface areas for **3a** and **4a** were calculated to be 201(305) and 125(224) m^2 g^{-1}, respectively. However, the adsorption isotherm for **3a** and **4a** revealed very low uptake of N_2 (77 K) (Figure 9a). The selectivity of CO_2 over N_2 may be due to size exclusion (kinetic diameter: 3.3 Å for CO_2 vs 3.64 Å for N_2)[1p] and the low kinetic energy of the N_2 molecules at 77 K resulting in N_2 molecules unable to effectively enter small pores.

The isotherms for H_2 adsorption/desorption were obtained at 77 K using an IGA analyzer according to previously described procedures.[6g,h] As shown in Figure 9b, **3a** reversibly adsorbs and desorbs H_2 at 77

(31) Zhao, X.; Xiao, B.; Fletcher, A. J.; Thomas, K. M. *J. Phys. Chem. B* **2005**, *109*, 8880.

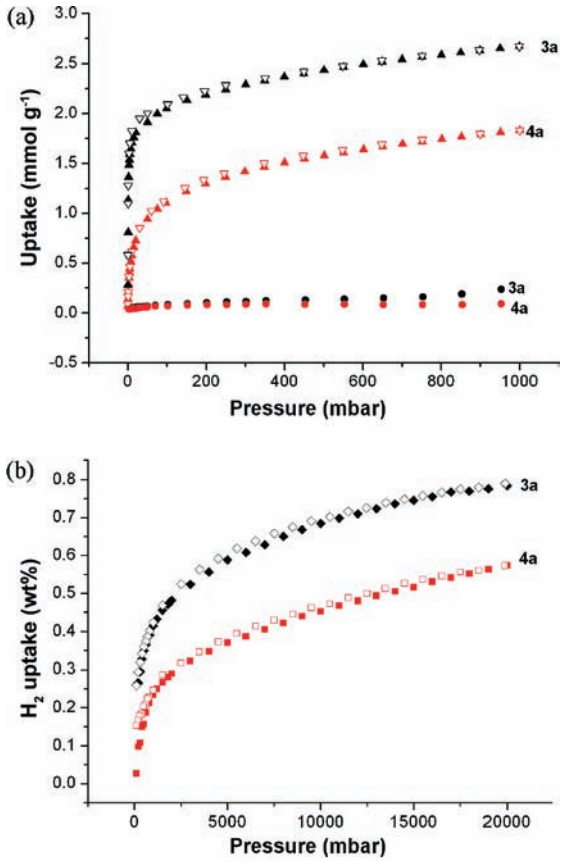

Figure 9. Absorption isotherms (a) N_2 (circles, 77 K) and CO_2 (triangles, 195 K) for **3a** (black) and **4a** (red); (b) H_2 absorption isotherm (77 K) for **3a** (black) and **4a** (red) (solid symbols for adsorption, open symbols for desorption).

K, a type-I adsorption behavior being observed. The H_2 uptake at 20 bar is 0.78 wt %, which is comparable to the values found for some carbon materials.[31] The Langmuir linear fitting of the H_2 adsorption data affords a maximum uptake of 0.87 wt %. The adsorbed H_2 density at 20 bar is 0.0326 g/cm^3, with respect to the solvent-accessible volume calculated from single-crystal data, notably lower than those observed for other 3D layer-pillared framework materials with α-Po topology (Supporting Information, Table S2).[6c,f,16,19a,22a−d,23f,32]

Sorption studies show the activated **4a** can adsorb 0.23 wt % H_2 at 77 K and 1 bar, increasing to 0.57 wt % H_2 at 20 bar (Figure 9b). These uptakes are comparable or superior to those observed for layered coordination frameworks under similar conditions.[23f,33] The absence of an absorption plateau before 20 bar shows further uptake can be expected at higher pressure. If H_2 molecules are considered to be stored in both intralamellar tubular channels and interlamellar voids (total free volume 26.3%), then the adsorbed H_2 density at 20 bar is half of the density of liquid H_2 (0.0708 g cm^{-3}).[34]

Conclusions

A new series of coordination polymers of different divalent metal cations [Zn(II), Cd(II) and Co(II)] have been assembled from the bent hfipbb^{2-} ligand under solvothermal conditions in the presence of auxiliary co-ligands. Complex **1** contains 2-fold 2D→2D parallel interpenetrated layers with binuclear Zn(II)-tetracarboxylate paddlewheel motifs as planar nodes and 1D double helical channels. In **3**, parallel interpenetrating helical layers composed of Zn(II)-tetracarboxylate paddlewheels and hfipbb^{2-} ligands are successfully extended by 1,4-bis(4-pyridyl)-2,3-diaza-1,3-butadiene (bpdab) pillars into a 3D α-Po microporous framework. However, the use of shorter 4,4′-bipyridine (4,4′-bipy) or 1,3-di(4-pyridyl)propane (dpp) as auxiliary ligands afforded 2D layered compounds **2** and **5**, both consisting of metal-hfipbb^{2-} ribbon-like chains connected together through bipyridyl ligands. Furthermore, the different bridging modes of hfipbb^{2-} ligands in **2** and **5** lead to different dispositions of the coordinated co-ligands around metal ions, giving as final products two significantly different (4,4) networks. The Cd(II) complex **4** represents a rare example in which metal centers are linked by carboxylate groups into infinite chains further joined together by double-stranded hfipbb^{2-} linkers to form a 2D network with tubular helical channels.

For the layered coordination polymers (**1**, **2**, **4**, and **5**) low accessible volumes (less than 27% of unit cell volume) were observed, because of close-packing of 2D layers or because of interpenetration of layers. Generally, these layered compounds show low thermal stability even under ambient conditions (e.g., **5**), but in the case of **4** which features tubular channels inside the layer, enhanced thermal stability of the guest-free framework is observed and its guest-free phase reversibly adsorbs and releases hydrogen at 77 K. The uptake of hydrogen at 20 bar is 0.57 wt %, among the highest values reported for layered frameworks. According to TGA, PXRD, and hydrogen adsorption studies, both **3** and **4** retain structural integrity and permanent microporosity upon evacuation of guest molecules although their overall porosity is relatively low.

Acknowledgment. This work was supported by Engineering and Physical Science Research Council (EPSRC), the European Research Council (ERC), the University of Nottingham, and the CVCP (ORS award to W.Y.). M.S. gratefully acknowledges receipt of a Royal Society Wolfson Merit Award.

Supporting Information Available: Additional structural figures and tables, and X-ray crystallographic information files (CIF) for compounds **1**−**5**. This material is available free of charge via the Internet at http://pubs.acs.org.

(32) (a) Chun, H.; Moon, J. *Inorg. Chem.* **2007**, *46*, 4371. (b) Chen, B.; Ma, S.; Hurtado, E. J.; Lobkovsky, E. B.; Zhou, H.-Z. *Inorg. Chem.* **2007**, *46*, 8490.

(33) (a) Kongshaug, K. O.; Fjellvåg, H. *Inorg. Chem.* **2006**, *45*, 2424. (b) Cabeza, A.; Gómez-Alntara, M. D. M.; Olivera-Pastor, P.; Sobrados, I.; Sanz, J.; Xiao, B.; Morris, R. E.; Clearfield, A.; Aranda, M. A.G. *Microporous Mesoporous Mater.* **2008**, *114*, 322.

(34) *CRC handbook of Chemistry and Physics*, 74th ed.; CRC Press: Boca Raton, FL, 1993.